PROCEEDINGS, TOUGH Symposium 2015
Lawrence Berkeley National Laboratory, Berkeley, California, September 28-30, 2015

# MODELING OF GAS MIGRATION THROUGH LOW-PERMEABILITY CLAY USING INFORMATION ON PRESSURE AND DEFORMATION FROM FAST AIR INJECTION TESTS

Rainer Senger[1], Enrique Romero[2], Paul Marschall[3]

[1] Intera Incorporated, Richland, WA 99354
[2] Department of Geotechnical Engineering and Geosciences, UPC, Barcelona, Spain
[3] Nagra, Wettingen, Switzerland
e-mails: rsenger@intera.com; enrique.romero-morales@upc.edu; paul.marschall@nagra.ch

## ABSTRACT

The characterization of gas migration through low-permeability clay formations has been a focus of R&D programs for radioactive waste disposal, which is also of great importance for shale-gas exploration, and cap-rock behavior of hydrocarbon reservoirs and $CO_2$ sequestration.

Laboratory tests on Opalinus clay cores from a shallow borehole in the Mont Terri Underground Research Laboratory (URL) and from a deep borehole in northern Switzerland included specific water and air injections tests, as well as oedometer and isotropic compression tests. For tests under different confining stress conditions, the rock compressibility was determined and the measured deformation was used to estimate changes in void ratio and to derive a relationship between void ratio and stress, and the corresponding changes in permeability as a function of changes in porosity.

For the shallow cores from Mont Terri, largely linear-elastic deformation associated with the gas injection test could be inferred and the change in void ratio was accounted for by the pore compressibility. The corresponding change in permeability was obtained from the results of the water tests, indicating a log-linear relation between permeability and porosity. The derived porosity change and corresponding change in permeability was implemented in the standard TOUGH2 code, which reproduced the measured gas test results using fitted water-retention data derived from laboratory measurements.

Similar injection tests performed on Opalinus clay cores from the borehole at greater depth showed overall similar behaviour, but at lower permeabilities, lower pore compressibilities and lower changes in porosity. These cases indicated non-linear behaviour which was implemented using an effective stress-dependent porosity change and associated change in permeability. In addition, the anisotropy associated with the bedding of the clay formation was considered by assuming different properties for "soft" and "hard' layers to account for storage capacity for the injected gas prior to gas breakthrough. The computed change in the overall porosity could be compared to the measured axial deformation during the gas injection test and was used for calibration of the parameters describing the relationship between the effective stress and porosity and the corresponding change in permeability and capillary pressure.

## INTRODUCTON

The National Cooperative for the Disposal of Radioactive Waste (NAGRA), Switzerland has developed a comprehensive program to characterize gas flow in the Opalinus Clay (OPA), one of the host rocks for a deep geological repository, through laboratory tests to determine the relevant hydraulic, geomechanical and two-phase properties, and to develop appropriate constitutive models through numerical analyses of the laboratory tests.

Understanding gas transport processes is an important issue in the assessment of radioactive waste repository performance and is the focus of paper. The actual gas migration mechanisms may entail standard two-phase flow or more complex mechanisms involving coupled two-phase geomechanical (Marschall et al., 2005) and possibly geochemical phenomena.

Laboratory tests on OPA cores from a shallow borehole (~300 m depth) in the Mont Terri Underground Research Laboratory (URL) and from a deep borehole (~800 m depth) in

northern Switzerland were described in detail by Romero et al. (2012), Romero and Gomez (2013) and Romero and Gonzalez-Blanco (2015).

## AIR INJECTION TESTS ON SHALLOW CORES

The air-injection tests were performed using a high-pressure triaxial cell, which was specifically designed to apply isotropic/ anisotropic stress states and to inject water at specified gradients or inject air at a controlled volume rate while measuring the outflow at a downstream chamber as well as the axial deformation. A detailed description of the experimental setup for the different tests and analyses is given in Romero et al., 2012a, b). A schematic of the test configuration is shown in Figure 1.

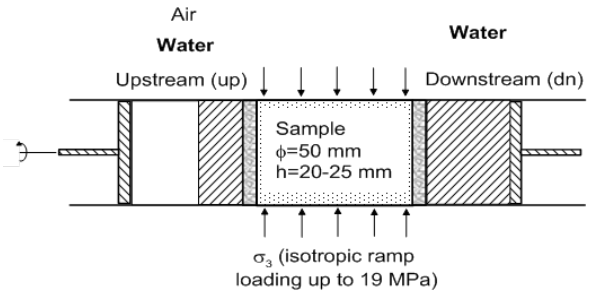


**A** Water permeability (starting from saturated state):
$P_{up}$=const.$_1$ (water); $P_{dn}$=const.$_2$ (water)
dV/dt (upstream and downstream volumes)

**B** Pressure pulse / decay air test:
Sudden $P_{up}$ (air); then $V_{up}$=const.$_1$ (air)
$P_{dn}$=const.$_2$ (water) (initial condition)
time evolution of $P_{up}$ and $V_{dn}$

Figure 1. Schematic of the test configuration for the water and air injection tests under isotropic and anisotropic stress states (Romero et al., 2012b).

For the water test preceding the air-injection tests, prescribed gradient conditions were used to determine the hydraulic conductivities. For water tests under different confining isotropic stress conditions, the measured axial deformation on low-height specimen was used to estimate the change in void ratio and to derive a relationship between void ratio and stress, and the corresponding change in permeability as a function of changes in porosity.

The time evolutions of air-injection pressure during the fast controlled volume-rate air injection test at 100 mL/min on two shallow OPA core samples with two bedding plane orientations are shown in Figure 2 together with the pressure / volume outflow response and axial deformation. The injection pressure increased up to about 12 and 13 MPa (depending on the orientation), followed by a shut-in and recovery period. For the flow parallel to bedding, outflow response was observed immediately after shut-in, corresponding to a sudden drop in the injection pressure, followed by a subsequent gradual decline. The pressure in the fixed-volume outflow chamber rapidly increased until reaching 2 MPa, when a constant pressure was maintained through a release valve.

For the flow perpendicular to bedding, the injection pressure increased to 12 MPa and remained relatively flat after shut-in (Figure 2). The outflow response is significantly delayed compared to the case with flow parallel to bedding. Only after the apparent gas breakthrough did the injection pressure show a steep decline. This test indicated gas migration into the sample for certain time prior to gas outflow (i.e., gas breakthrough) at an injection pressure of 12 MPa which is significantly below the fitted van Genuchten (1980) capillary air-entry parameter of 18 MPa from the water retention data (Romero et al., 2012a).

The axial deformation revealed two different deformation regimes. For the test parallel to bedding (Figure 2), the initial pressure increase shows axial deformation at negative values indicating expansion. During the early period after shut-in, the pressure slightly decreased but the axial strain continued to increase. Afterwards, as the pressure continued to decrease, the axial deformation reversed indicating compression as the effective stress increased.

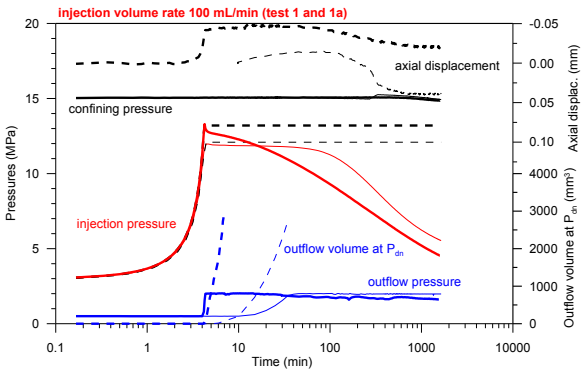


Figure 2. Measured pressures at the injection and outflow sides together with outflow data and axial displacements for the air injection test parallel (thick lines) and normal (thin lines) to bedding for shallow OPA core sample (from Romero et al., 2012a, b).

For the gas test with flow normal to bedding (Figure 2), the axial deformation indicates a similar pattern, although no measurements were available during the early injection period. During the early period after shut-in, very little change in pressure occurred, whereas the axial deformation went negative indicating expansion. At late time, the axial deformation reversed as the pressure decline steepened indicating compression. The axial deformation, reflecting the changes in void ratio, indicates that during the injection period expansion and a corresponding increase in void ratio occurred associated with gas migration into the pore space of the core sample and effective stress decrease due to pore pressure increase. This expansion continued beyond the shut-in as the gas pressure front propagated into the sample causing the fluid pressure to increase and the effective stress to decrease. At late time after the pressure in the outflow chamber started to increase, the injection pressure declined and the effective stress increased, indicating compression.

## Modeling Approach

For the analysis of the air-injection tests, the test configuration was implemented in a numerical model using the two-phase flow code TOUGH2 (Pruess et al., 1999). In a first step, the measured results in terms of permeability, porosity, and pore compressibility, as well as the two-phase parameters derived from the water retention data were used as initial estimates for the inverse modeling using iTOUGH2 (Finsterle, 2007). The resulting simulations could not reproduce well the observed injection-pressure responses over the entire test and outflow responses for both air-pulse tests (parallel and normal to bedding). Moreover, the estimated parameters were significantly different from those derived from the measured retention curves and from the water tests (Senger et al., 2014).

A revised approach was then used taking into account the relations between void ratio and stresses (Romero et al., 2012a). Changes in porosity are accounted for in the standard TOUGH2 code through the pore compressibility, whereas the potential change in permeability is not. Assuming largely linear-elastic deformation associated with the gas injection test, the inferred change in void ratio can be accounted for by the pore compressibility. With the confining stress kept constant at 15 MPa during the air pulse injection tests, the variation in effective stress can be related to the variation in pressures. In TOUGH2 the effect of compressibility is accounted for by the change in porosity ($d\phi$) in response to a change in fluid pressure ($dP$) as:

$$d\phi = \phi C_p dP \qquad (1)$$

The corresponding change in permeability was obtained from the results of the water tests, indicating a log-linear relation between permeability and porosity (Romero et al., 2012a, b). For two-phase flow, the change in porosity/permeability also affects the capillary pressure, which is accounted for by the Leverett function (Leverett, 1941).

For the revised analysis only forward simulations were performed using the two-phase parameters based on the measured retention curve data and the estimated permeability from the water test (Table 1). The results of the simulations for the air-injection tests parallel and perpendicular to bedding planes are shown in Figure 3. The simulation, incorporating the coupling between the changes in porosity, due to pore compressibility associated with the increased pore-pressure, and the corresponding permeability changes reproduced both the injection pressure response and the outflow pressure response. The peaks of the outflow response are

due to the fact that the effect of the release valve at 2 MPa was arbitrarily set at a certain time after the gas breakthrough response.

Table 1. Model input parameter (shallow OPA)

| | Test 1a (parallel) | Test 1 (normal) |
|---|---|---|
| Permeability: k ($m^2$)[a] | 1.4E-19 | 4.3E-20 |
| Porosity [-][a] | 0.20 | 0.18 |
| Pore compress. $C_p$ [1/Pa][a] | 2.0E-08 | 1.5E-08 |
| van Genuchten: $P_0$ [Pa][b] | 18.0E+6 | 18.0E+6 |
| van Genuchten; n[b] | 1.67 | 1.67 |
| Res. water saturation: $S_{lr}$[c] | 0.01 | 0.01 |
| Res. gas saturation: $S_{gr}$[c] | 0 | 0 |
| Initial saturation ($S_w$)[c] | 1 | 1 |

[a]measured, [b]fitted to WRC, [c]assumed

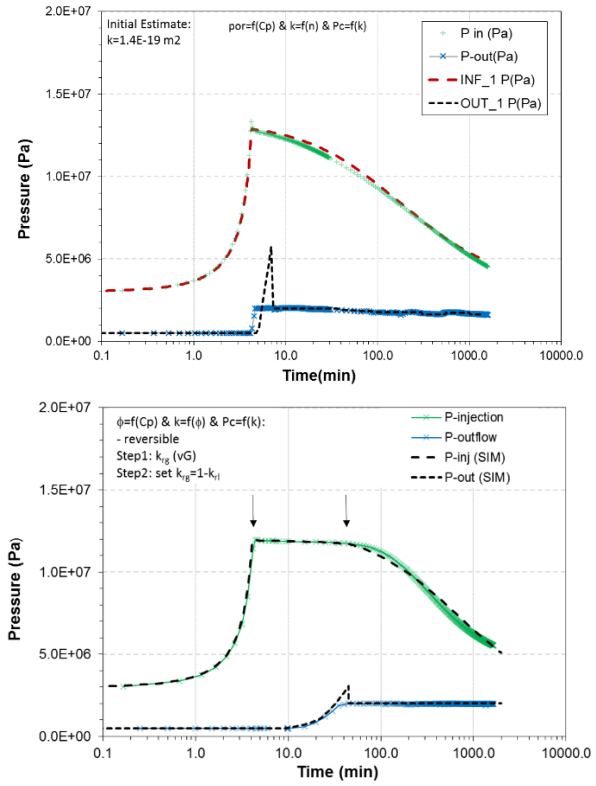


Figure 3. Simulated (dashed lines) and measured (solid lines) pressures for air-injection tests for flow parallel to bedding) (top), and for flow perpendicular to bedding (bottom) (modified from Senger et al., 2014); the arrows note the times for the profiles in Figure 4.

Figure 3 shows that the outflow response for the test perpendicular to bedding is significantly later than for the test parallel to bedding. That is, gas continues to migrate into the expanding pores prior to the breakthrough response. One can assume that preferential gas pathways are established resulting in higher gas mobility and less phase interference. This is represented by a Grant model for the gas relative permeability (e.g., $k_{rg} = 1\text{-}k_{rl}$), which produced the more rapid injection pressure decline following the gas breakthrough.

The computed changes in permeability due to the changes in porosity within the core during the air-injection test are shown together with the pressure and saturation profiles in Figure 4. After gas injection stopped (after 4.17 min), the gas pressure profiles indicate the gas front migrating into the sample. The computed permeability increases from the initial 4.3E-20 $m^2$ to 2.5E-19 $m^2$ corresponding to an increase in porosity from 0.18 to about 0.21 which, in turn, correlates to the axial displacements, shown in Figure 2. After 45 minutes - at about gas breakthrough - the increased permeability extends across the entire core corresponding to the maximum expansion of the core sample (Figure 2).

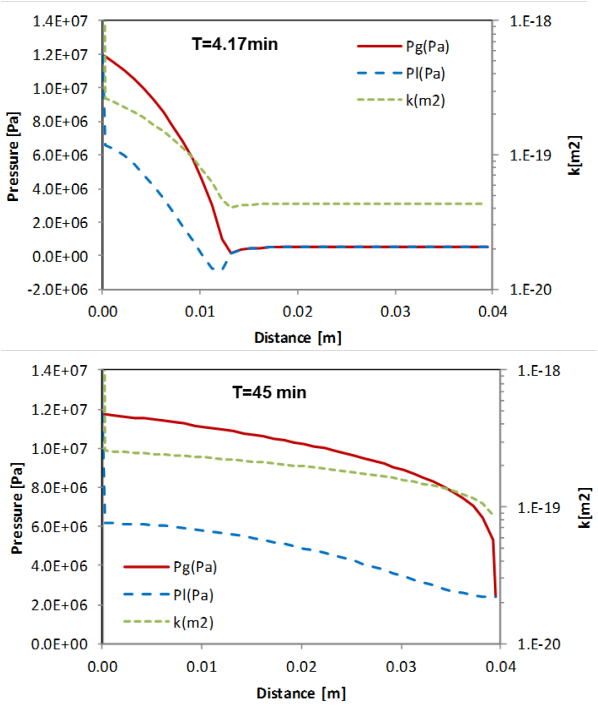


Figure 4. Computed vertical profiles of gas pressure (Pg), liquid pressure (Pl) and permeability (k) throughout the core height (perpendicular to bedding) after 4.17 min (top) and 45 min (bottom).

## AIR INJECTION TESTS ON DEEP CORES

The air-injection tests on OPA core samples from a depth of about 800 m in the Schlattingen borehole in northern Switzerland showed overall similar responses (Figure 5) as those from the shallow borehole at Mont Terri (Figure 2). Only cores perpendicular to bedding were available from the deep borehole. Similar to the shallow analyses, a series of complementary tests were performed preceding the air injection tests, which included compression tests, water permeability tests, and water retention measurements which are described in detail in Romero and Gomez (2013).

The air injection test in Figure 5 was performed under isotropic stress conditions of 15 MPa. Compared to the shallow tests procedure, the deep tests measured the actual outflow volume increase instead of the pressure increase which was limited to a maximum of 2 MPa. Even though the overall response was similar, the deep cores indicated a significantly later outflow response (only after more than 100 min) compared to the shallow air injection test (Figure 2). Also, the injection pressure following shut-in after 4.2 minutes shows a more distinct decline, indicating gas flow into the sample. That is, the injected gas has to accumulate in the core until outflow response occurs.

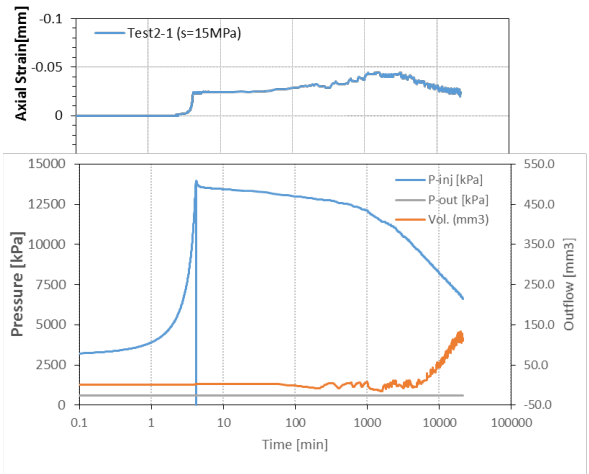


Figure 5. Measured pressures at the injection side and outflow volumes at the downstream side together with axial displacements for the air injection test perpendicular to bedding for a deep OPA core sample (after Romero and Gomez, 2013).

On the other hand, the maximum axial expansion of the deep core during the air injection test is similar to that of the shallow core (Figure 2). Moreover, the estimated compressibility from the compression tests and initial porosity is much lower than for the deep core sample. Potential non-reversible changes in the pore volume were indicated by the measured pore size distributions before and after the air-injection tests, changing to a bi-modal pore size distribution with new "pores" having two orders of magnitude higher entrance pore size (Romero and Gonzalez-Blanco, 2015).

Table 2 summarizes the properties of the deep OPA core sample, indicating also higher suction with a fitted van Genuchten parameter $P_0$ of 34 MPa (Romero and Gomez, 2013). This information together with the additional parameters is used as input for the numerical modeling described below.

Table 2. Model input parameter (deep OPA)

| | **Test 2-1 (normal)** |
|---|---|
| Permeability: k ($m^2$)[a] | 1.3E-21 |
| Porosity: $\phi_r$ [-][a] ($\phi_o$) | 0.1 (0.15) |
| Pore compress. $C_p$ [1/Pa][a] | 1.0E-09 |
| van Genuchten: $P_0$ [Pa][b] | 34.0E+06 |
| van Genuchten; n[b] | 1.58 |
| Res. water saturation: $S_{lr}$[c] | 0.01 |
| Res. gas saturation: $S_{gr}$[c] | 0 |
| Initial saturation ($S_w$)[c] | 1 |
| Coefficient: $\alpha$ [1/Pa] (soft) | 1.0, (0.6) |
| Factor for k-$\phi$: c | 10 |
| Enhancement factor for $k_{rg}$ | 10 |
| [a]measured, [b]fitted to wrc, [c]assumed | |

### Modeling Approach

The observed responses from the deep core sample suggest more complex phenomena of gas migration through the clay implying non-linear behavior associated with pathway dilation.

For this analysis, the layering of the OPA is explicitly implemented by alternating layers of different material properties. This allows preferential gas migration into "softer" interlayers having somewhat higher permeability before migrating to the next interlayer. The gas migra-

tion front in the axial direction is thus retarded and provides greater storage capacity for the observed gas flow into the sample prior to gas breakthrough.

In addition, the potential changes in hydraulic properties are described as a function of effective stress, using the empirical function given by Rutqvist et al. (2002):

$$\phi = \phi_r + (\phi_0 - \phi_r)e^{-\alpha\sigma'} \qquad (2)$$

where $\phi_0$ is zero effective stress porosity, $\phi_r$ is the residual porosity at high effective stress, and the exponent $\alpha$ is a rock parameter. The addition of the residual porosity $\phi_r$ results in a relatively steep increase in porosity in the low effective-stress range. An associated exponential function for permeability as a function of porosity is given by (Rutqvist et al., 2002):

$$k = k_0 e^{c(\frac{\phi}{\phi_0}-1)} \qquad (3)$$

where $k_0$ is the initial reference permeability and c is a rock specific parameter (Table 2). Figure 6 (top) shows the computed effective stress, based on the total stress of 15 MPa, and the injection pressure response through time. The computed porosity as a function of effective stress assumed a parameter $\alpha$ = 0.6 $Pa^{-1}$ for the 'soft' interlayer (Table 2). The computed porosity shows a steep increase when the peak injection pressure and lowest effective stress is reached (Figure 6 top), which compares with the steep volume expansion indicated by the axial displacement (Figure 5).

The corresponding porosity and permeability as a function of effective stress (Figure 6, bottom) show an exponential increase with decreasing effective stress. The permeability depends largely on the coefficient 'c' in Equation (3), which was set to 10 (Table 2) in Figure 6 (bottom).

Compared to the previous air injection tests on the shallow OPA cores (Figure 1), the boundary condition on the outflow was changed. In order to directly simulate the volume increase, a relatively high pore compressibility was assigned to the element representing the outflow chamber.

Any mass flow into the outflow chamber and corresponding pressure increase is represented by an increase in porosity, which can be converted to a volume increase for comparison with the measured volume increase of the outflow chamber.

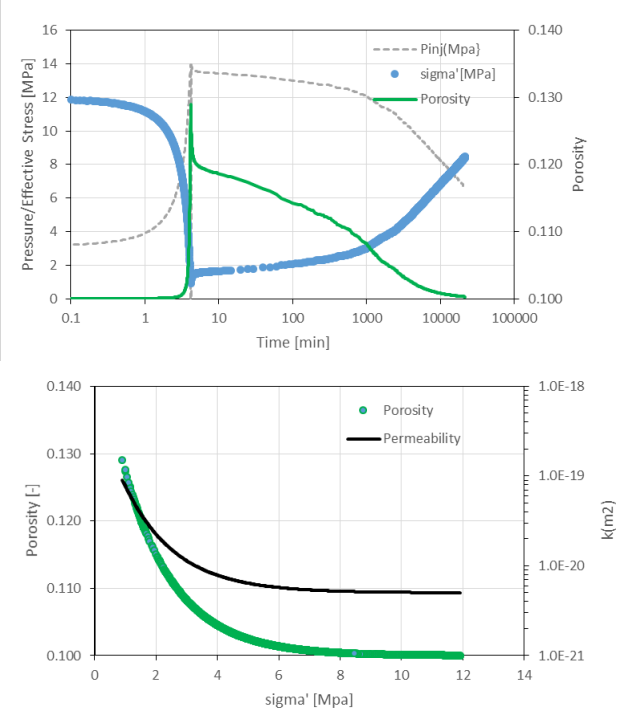


Figure 6. Injection pressure, effective stress and computed porosity based on Equation 2 (top) and corresponding permeability based on Equation 3 (bottom), representing the maximum changes at the upstream boundary of the core (see Figure 4).

In order to more realistically represent the bedding of the OPA core, a 2D random heterogeneous porosity/permeability field was generated to reproduce the typical anisotropy of the OPA formation. For the soft interlayers, the porosity increase was estimated using an $\alpha$ parameter of 0.6 $Pa^{-1}$, compared to the hard layers for which the parameter was set to 1 $Pa^{-1}$. An enhancement factor for the gas relative permeability has been also considered to account for the higher mobility when a gas path has developed (instead of arbitrarily setting $k_{rg}=1-k_{rl}$).

The results for this simulation are shown in Figure 7 in terms of time evolutions of the

simulated injection pressure (top) and the computed outflow volume (bottom). The simulated injection pressure shows relatively little decline following the shut-in and a later pressure recovery compared to the measured injection pressure. At late time, the pressure recoveries are similar. On the other hand, the computed outflow volume shows an earlier increase compared to the measured response, indicating an earlier gas breakthrough but at a similar rate. The comparison suggests a somewhat higher gas flow into the sample prior to the gas breakthrough, requiring an increase in gas permeability and associated accumulation of the injected air in the dilated pathways without a connection to the outflow boundary.

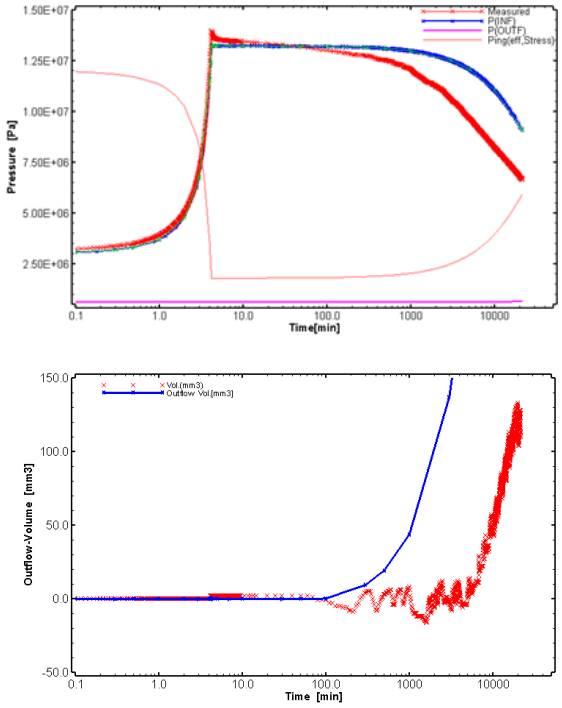


Figure 7. Simulated and measured injection pressures (top), and computed outflow volume increase for comparison with measured outflow volume.

The system response is depicted in Figure 8 in terms of the spatial distribution of gas saturation, porosity, and gas permeability after 100 minutes, when the gas front reaches the outflow boundary at the top. The gas saturation indicates relatively large variability due to the permeability variations within layers and between layers.

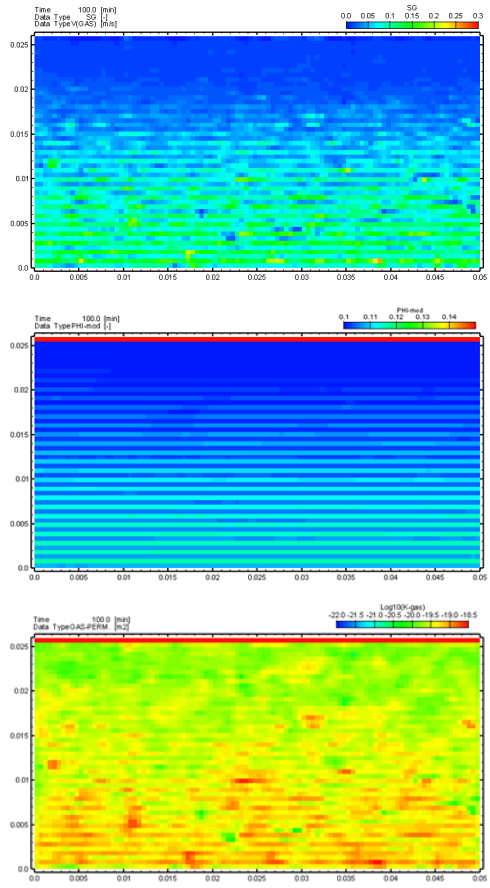

Figure 8. Simulated distribution of Sg (top), porosity (middle), and gas permeability (bottom) after 100 min.

## SUMMARY AND OUTLOOK

The detailed analyses of laboratory experiments on Opalinus Clay cores were used to develop a conceptual and numerical model for simulating two-phase flow of gas through a low-permeability clay formation. The specific test configuration of the fast air-injection tests complemented by isotropic compression test, water permeability test, and water retention measurement provided consistent data sets which are enhanced by the measured displacement during the air-injection tests. The air-injection test responses for the shallow OPA cores could be reasonably well reproduced assuming standard two-phase flow accounting for the change in porosity associated with the measured pore compressibility and for the change in permeability and capillary pressure. The results of the air-injection tests of the deep OPA cores indicated overall similar behavior in terms of

pressure responses and measured axial displacement as the shallow cores. However, the implied changes in porosity and permeability required more complex processes associated with creation of additional pore space through pathway dilation. Existing models of stress-dependent porosity/permeability changes could not reproduce both the injection pressure response and outflow response, even when accounting for the layered structure of the OPA, assuming soft and hard layers. These models are limited in that the change in porosity is uniform for all pores. In reality, only certain pores or pore-size fraction may undergo micro fissuring producing oriented higher-permeable pathways. Such phenomena will be evaluated in further studies.

## ACKNOWLEDGMENT

This study has been performed under contract from the National Cooperative for the Disposal of Radioactive Waste (NAGRA), Switzerland.

## REFERENCES

Finsterle, S., *ITOUGH2 User's Guide*, Report LBNL-40040, Lawrence Berkeley National Laboratory, Berkeley, Calif., 2007.

Leverett, M.C., Capillary behaviour in porous solids, *Transactions of the AIME* 142, 159–172, 1941.

Marschall, P., Horseman, P., and T. Gimmi, Characterization of gas transport properties of the Opalinus Clay, a potential host rock formation for radioactive waste disposal, *Oil and Gas Science and Technology*, 60, 121-139, 2005.

Pruess, K., C. Oldenburg, and G. Moridis, *TOUGH2 User's Guide, Version 2.0*, Report LBNL-43134, Lawrence Berkeley National Laboratory, Berkeley, Calif., 1999.

Romero, E., Senger, R., and Marschall, P., Air injection laboratory experiments on Opalinus Clay, Experimental Techniques, Results and Analyses: 3rd EAGE Shale Workshop, Barcelona, 23-25 January, 2012a.

Romero, E., Senger, R., Marschall, P., and Gómez, R., Air tests on low-permeability claystone formations. Experimental results and simulations, *in* Multiphysical Testing of Soils and Shales. L. Laloui & A. Ferrari (eds.). Springer-Verlag, Berlin: 68-83, 2012b.

Romero, E., and Gomez, R., Water and air permeability tests on deep core samples from Schlattingen SLA-1 borehole; Material characterization and experimental set-up. Compressibility on loading, water permeability and air injection results, NAGRA Report NAB 13-51, 2013.

Romero, E. and Gonzalez-Blanco, L., Complementary water and air permeability tests on core samples from Schlattingen SLA-1 borehole, NAGRA Report NAB 15-06, 2015.

Senger, R.K., E. Romero, A. Ferrari, and P. Marschall, Characterization of gas flow through low-permeability claystone: Laboratory - experiments and two-phase flow analyses, in Norris et al., Clays in natural and engineered barriers for radioactive waste confinement, Geological Society, London, Special Publication, 400, 2014.

Rutqvist J, Wu Y-, Tsang C-, Bodvarsson G., A modeling approach for analysis of coupled multiphase fluid flow, heat transfer, and deformation in fractured porous rock, *Int J Rock. Mech Min Sci* 39, 429–442, 2002.

van Genuchten, M.Th. A closed-form equation for predicting the hydraulic conductivity of - unsaturated soils, *Soil Sci. Soc.Am. J.,* 44, 892 – 898, 1980.